ACS APPLIED BIO MATERIALS

www.acsabm.org Article

Cancer Cell Detection on the Surface of Top-Gated Monolayer Graphene via Raman Spectroscopy

Sitansu Sekhar Nanda, Sandeep Kaushal, Yong Shin, Kyusik Yun, Seong Soo A. An, K. P. S. S. Hembram, Georgia C. Papaefthymiou, and Dong Kee Yi*

Cite This: *ACS Appl. Bio Mater.* 2021, 4, 1493−1498 Read Online

ACCESS | Metrics & More | Article Recommendations | Supporting Information

ABSTRACT: A label-free biosensor is described based on the Raman spectroscopic signatures of monolayer graphene, which are modified in the compartment of cancer cells because of electron−phonon coupling in monolayer graphene. Specifically, the Raman spectra of electrostatically gated monolayer graphene on SiO_2/Si substrates, in the voltage range from 0 to 5 V, were studied in the absence and the presence of cancer cells. Density functional theory simulations afforded a correlation between cancer cells and the observed Raman spectra, through the regulation of the intensities of the G and 2D Raman vibrational modes with applied voltage. The C−H and N−H bonds of phenylalanine enabled the detection of this biosensing activity. Significantly, this detection can be carried out even in the absence of cancer cell-culturing steps.

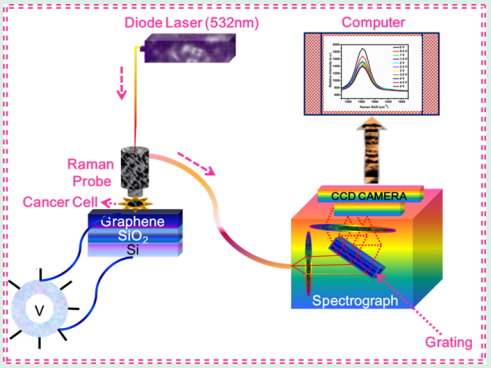

KEYWORDS: *Raman spectroscopy, graphene, cancer cell, biosensor, DFT*

INTRODUCTION

Graphene[1−5] has promoted many basic studies in physics and potential applications in nanotechnology. In the healthcare sector, many applications are being investigated such as graphene-mediated photothermal therapy of cancer,[6] gene transfection,[7] magnetic resonance imaging,[8] etc. Because of its one atom thickness and ambipolar nature, graphene−neoplastic activity induces necrosis of monocytic cancer cells.[9,10] We focus on the discernment of the interaction of cancer cells with graphene, which is fundamentally not well understood.

Label-based biosensors require the addition of reagents and the performance of washing steps carried out cautiously.[11] In contrast, label-free methods offer simple and rapid measurement.[11] Real-time monitoring of binding reactions and kinetic parameters of molecular recognition have been accomplished by label-free methods.[12] A label-free method includes minimized sample processing, and fewer resources for assay development.[13] For hit finding/validation, screening the interaction of cells with drugs and accessing difficult target classes are achieved using a label-free biosensor.[14]

Recently, label-free sensing methodologies utilizing techniques such as infrared spectroscopy,[15] Raman spectroscopy,[16,17] mass spectrometry,[18] random amplified polymorphic DNA,[19] and the field effect transistor[20] have been employed for the detection and identification of cancer cells. Of late, straightforward colorimetric urinary data can be obtained by using multifunctional protease nanosensors.[21] Their rapid response to a disease microenvironment makes data available within 1 h. Among all label-free methods mentioned above, Raman spectroscopy is a powerful and nondestructive technique and hence widely acceptable. Raman spectroscopy affords an attractive tool in diagnostics of in vivo cancer cells,[22] basal cell carcinoma,[23] circulating tumor cells,[24] neoplastic hematopoietic cells,[25] and the specific detection of Gram +ve and Gram −ve bacterial strains.[26] With suitable care, even isolated cancer cells can be detected and characterized with Raman spectroscopy.[27] It links lineaments of these approaches up to the specificity of the Raman signal.

Keisham et al. analyzed the detection and the activity of cancer cells supported on graphene with Raman mapping and attributed it to the hole-doping mechanism.[28] Although surface-enhanced Raman spectroscopy (SERS) has occasionally been used to detect cancer cells, the detection mechanism has not yet been elucidated.[29] With electrostatically gated monolayer graphene, a significant change in charge carrier density occurs because of graphene's quantum capacitance.[30,31]

Herewith, we present unusual vibrational modes within the gaps between monolayer graphene and cancer cells through extreme atomic-scale field localization. Simultaneously, the-

Received: October 23, 2020
Accepted: December 17, 2020
Published: January 11, 2021

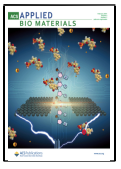

https://dx.doi.org/10.1021/acsabm.0c01377
ACS Appl. Bio Mater. 2021, 4, 1493−1498

oretical methods are employed to study this extreme atomic-scale field. We show that this protocol can be used for detection of six unique types of cancers without tedious cell culturing steps, and we believe we can further expand this method to recognize cancers for home medical use and clinical diagnosis. Here, we predict the SERS signal of the phenylalanine molecule, which is widely used in SERS measurements because of its high sensitivity, high-quality signals, and excellent performance. Based on the quantum mechanics data of electronic and vibrational structures for thousands of ab initio molecular dynamics conformations, we will apply the machine learning protocol. We predict the Raman frequency and intensity of each dominant vibrational mode of cancer cells with its mode-specific descriptor. The final density functional theory model is successfully applied to predict SERS of phenylalanine in the presence of electric fields, and other molecular surfaces, suggesting good transferability.

RESULTS AND DISCUSSION

Physical characterization of a monolayer graphene film grown by chemical vapor deposition is given in Figure S1. Scanning electron microscopy and optical microscopy images are presented in Figure S1A,B, respectively, for the full growth monolayer graphene film. Atomic force microscopy imaging confirmed the fully grown monolayer graphene on SiO_2 with a 0.36 ± 0.05 nm thickness using cross-sectional analysis in Figure S1C.

All subsisting spectroscopic techniques require cultivation of cancer cells prior to detection, a time-consuming process. Exploration of alternate detection approaches for cancer cell identification without cultivation is desirable. Hence, the development of an effective, low-cost protocol to investigate the anticancer properties of graphene, which can have a significant environmental and health-care impact, is of paramount importance. The proposed method can lead to reliable results with feasibility of detection at low cancer-cell concentrations (20 μL suspension ~10^3 cancer cells). To better understand the activation of phenylalanine (which is a major constituent in cancer cells[32]), we examined the concerned Eigen vibrational modes through first-principles calculations. Signatures of the symmetric stretching frequencies shown in Figure 1 are observed in the Raman spectra.

It relates phenylalanine vibrational modes to various cancer types, such as breast, oral, prostate, esophageal, and lung tissue samples.[32] González-Solís et al.[33] proved that the stage of breast cancer interrelated with phenylalanine intensity (1002 cm^{-1}). In the present work, we affirm the Raman peak associated with phenylalanine can be a fingerprint for the detection of cancer cells. The Raman spectra of the aromatic amino acid phenylalanine and its C−H and N−H stretching are shown in Figure 2. It is well known that the G and 2D bands of graphene occur at ~1580 and 2700 cm^{-1}, respectively.[34] Without the presence of a physical interaction, such as energy exchange, it cannot shift the G band and 2D band of graphene. It introduces a similar observation in Figure 2.

Dissimilar surface electron states related to cancer cells in the D, G, and 2D bands are shown in Figure 3 and Table 1. Cancer cell membranes can change the Fermi level of monolayer graphene by an electron transfer mechanism.[26] Radical alteration took place after the deposition of cancer cells on monolayer graphene. Phenylalanine as the fingerprint of CT-26, SCC-7, CCD-841, HEK293, N9, HepaRG, HepG2,

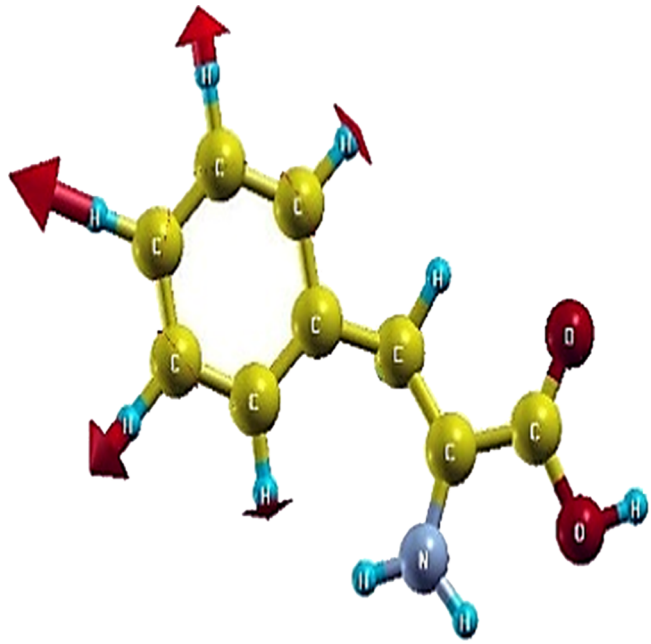

Figure 1. Symmetric stretching frequency of the C−H bond (2825, 2955, 3127, and 3210 cm^{-1}) and the N−H bond (3450 cm^{-1}) in the aromatic ring of phenylalanine (H-sky blue, C-yellow, N-gray, and O-red).

MDAMB 231, and MDAMB 468 cells can be distinguished. In the absence of cancer cells, there is nearly equal intensity observed for the G, 2D, and D bands (Figures S7−S9).

The simulation unravels the bonding characteristics of the constituents (partial) of cancer cells, that is, the C−H and the N−H bonds. The nature of the C−H bonds is revealed by various Raman peaks, confirmed by phonon Eigen vectors assigned to relevant frequencies and categorized into two groups, that is, aliphatic and aromatic (Figure 4). In aliphatic, the C−H bond strength of the $-CH_2$ group appears at a lower frequency ~2825 cm^{-1} compared to the $-CH_3$ group with a frequency of ~2955 cm^{-1}. This shows that the C−H bond of $-CH_2$ is less stiff (bond length 1.117 Å) than that of the $-CH_3$ group (bond length 1.095 Å). We clearly observe these features from the Raman peaks of SCC-7 cells (Figure S2) (2955 cm^{-1}). However, the colon cancer cells show a major peak at (~2825 cm^{-1}). The C−H bond strength from the aromatic group shows the peak at ~3127 cm^{-1} (much stiffer bond strength, 1.090 Å) which is revealed at ~3210 cm^{-1} from all the cancer cells (Figures 4A and S2−S10). With MDAMB 231 cells, the 2825 and 3127 cm^{-1} peaks with dissimilar intensity were observed (Figure S3). In another study of MDAMB using 468 cells, dissimilar intensity peaks at 2825 and 3210 cm^{-1} were observed (Figure S4). Although both the MDAMB 231 and MDAMB 468 cell samples were breast cancer cells, different bands are viewed because of dissimilar culture procedures. The MDAMB 468 cells were cultured and stored in the presence of 5% CO_2, while the MDAMB 231 cells were processed in the absence of CO_2. From a biological point of view, the MDA-MB-231 cell expression is related to mammary cancer stem cells, such as the CD44 + CD24-/low phenotype. The MDA-MB-231 cells are associated with the epithelial−mesenchymal transition.[35,36] These features are not shared with MDA-MB-468. Thus, they exhibit different phenotypic and molecular behavior, as observed in their sensing methods (Figures S3−S5). C−H and N−H stretching

https://dx.doi.org/10.1021/acsabm.0c01377
ACS Appl. Bio Mater. 2021, 4, 1493−1498

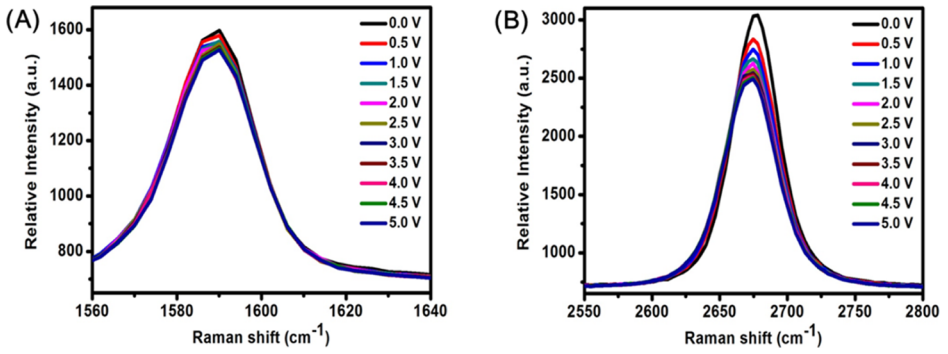

Figure 2. (A) Raman G band of monolayer graphene with a voltage variation from 0 to 5 V. Standardized intensity noted in the case of the G band at 1585 cm^{-1}. (B) Raman 2D band of monolayer graphene with a voltage variation from 0 to 5 V. Standardized intensity mentioned in the case of the 2D band at 2680 cm^{-1}.

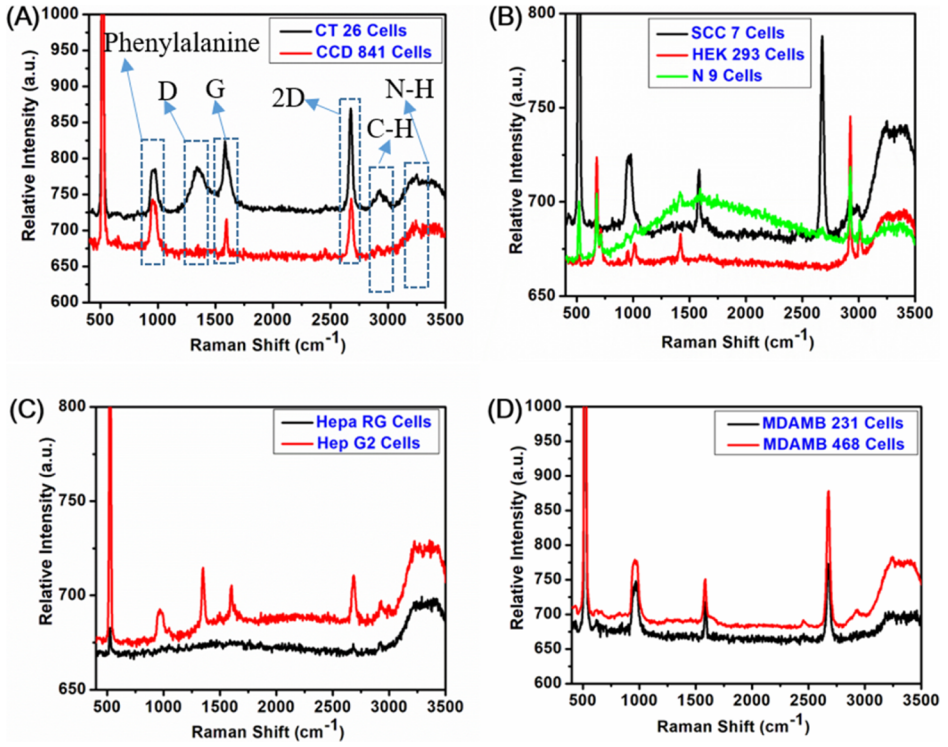

Figure 3. Dissimilar peaks of (A) CT-26, CCD-841 (B) SCC-7, HEK293, N9 (C) HepaRG, HepG2 (D) MDAMB 231, and MDAMB 468 cells. Peak at 1000 cm^{-1} is attributed to phenylalanine. C−H stretching bands are seen at 2825 and 3210 cm^{-1}. Simultaneously, the G band (1585 cm^{-1}), 2D band (2700 cm^{-1}), and D band (1350 cm^{-1}) are seen in this figure.

is clearly visible in liver (HepaRG) cells (Figure S5) (2825 cm^{-1}) and invisible in liver (HepG2) cancer cells (Figure S6). Similarly, the N−H bond shows a peak at a frequency of 3450 cm^{-1} (Figures 4B, S2−S5, and S7−S10). The higher N−H stretching signal is because of the stiffer bonding (1.012 Å) compared to the C−H bond (1.090 Å). It assigns the other prominent peaks to G (~1585 cm^{-1}), D (~1350 cm^{-1}), and 2D (~2700 cm^{-1}) bands.

The above data inform about which atoms are present, and about the way they link them. The topology of a molecule affects its carcinogenic activity in living organisms and plays an important role in causation of cancer.[37] Thus, the deformation of the C−H and N−H bonds is associated with different cancer cells.

Theoretical scaling of the C−H bond-stretching frequency (ω) versus the total molecular mass (m) of the system is shown in Figure 4A. C−H bond stretching ranges from 2750 to 3150 cm^{-1}. Theoretical scaling of the N−H bond-stretching frequency (ω) versus the total molecular mass (m) of the system is shown in Figure 4B. N−H bond stretching ranges from 3200 to 3500 cm^{-1}. All the experimental results well match with the theoretical results. Thus, further technical development of Raman spectroscopy can play an important role in label-free biosensing applications.

In this article, we have shown detection feasibility for six types of cancer, using the proposed label-free biosensor. This method can be further expanded by preparing typical cancer markers, which can be indicators of every single type of cancer. It can be used in the proposed method with a commercial, portable Raman spectrometer for creating miniaturized cancer-detecting devices for personalized care and in-field use.

https://dx.doi.org/10.1021/acsabm.0c01377
ACS Appl. Bio Mater. 2021, 4, 1493−1498

Table 1. Dissimilar Peaks of CT-26, SCC-7, CCD-841, HEK293, N9, HepaRG, HepG2, MDAMB 231, and MDAMB 468 Cells[a]

	G band	2D band	phenylalanine band	C−H band	N−H band
graphene (contrrol)	1585 cm^{-1} with similar intensity	2680 cm^{-1} with similar intensity	absent	absent	absent
CT-26 cells	1585 cm^{-1} with dissimilar intensity	2680 cm^{-1} with dissimilar intensity	1000 cm^{-1} with dissimilar intensity	2825 and 3210 cm^{-1} with dissimilar intensity	absent
MDAMB 231 cells	1585 cm^{-1} with dissimilar intensity	2680 cm^{-1} with dissimilar intensity	1000 cm^{-1} with dissimilar intensity	2825 and 3127 cm^{-1} with dissimilar intensity	3450 cm^{-1} with dissimilar intensity
MDAMB 468 cells	1585 cm^{-1} with dissimilar intensity	2680 cm^{-1} with dissimilar intensity	1000 cm^{-1} with dissimilar intensity	2825 and 3210 cm^{-1} with dissimilar intensity	3450 cm^{-1} with dissimilar intensity
SSC-7 cells	1585 cm^{-1} with dissimilar intensity	2680 cm^{-1} with dissimilar intensity	1000 cm^{-1} with dissimilar intensity	2825, 2955 and 3210 cm^{-1} with dissimilar intensity	3450 cm^{-1} with dissimilar intensity
HepaRG cells	1585 cm^{-1} with dissimilar intensity	2680 cm^{-1} with dissimilar intensity	1000 cm^{-1} with dissimilar intensity	2825 $cm^{-1}$with dissimilar intensity	3450 cm^{-1} with dissimilar intensity
CCD 841 cells	1585 cm^{-1} with dissimilar intensity	2680 cm^{-1} with dissimilar intensity	1000 cm^{-1} with dissimilar intensity	2825 and 3210 cm^{-1} with dissimilar intensity	3450 cm^{-1} with dissimilar intensity
HEK293 cells	1585 cm^{-1} with dissimilar intensity	2680 cm^{-1} with dissimilar intensity	1000 cm^{-1} with dissimilar intensity	2825 and 3127 cm^{-1} with dissimilar intensity	3450 cm^{-1} with dissimilar intensity
N9 cells	1585 cm^{-1} with dissimilar intensity	2680 cm^{-1} with dissimilar intensity	absent	2825 and 3127 cm^{-1} with dissimilar intensity	3450 cm^{-1} with dissimilar intensity
HepG2 cells	1585 cm^{-1} with dissimilar intensity	absent	absent	absent	3450 cm^{-1} with dissimilar intensity

[a]The peak at 1000 cm^{-1} is attributed to phenylalanine. C−H and N−H stretching bands are seen. Simultaneously, the G (1585 cm^{-1}), 2D (2700 cm^{-1}), and D (1350 cm^{-1}) bands observed in this figure.

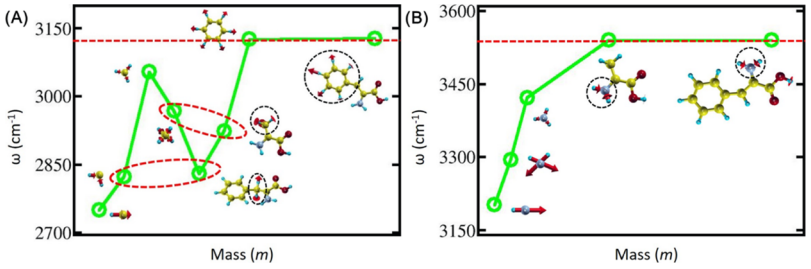

Figure 4. (A) Theoretical scaling of the C−H bond-stretching frequency (ω) vs the total molecular mass (m) of the system. (B) Theoretical scaling of the N−H bond-stretching frequency (ω) vs the total molecular mass (m) of the system.

CONCLUSIONS

We have described a label-free biosensor that permits the identification of cancer cells without cell cultivation. We have examined the electrochemical properties of monolayer graphene in order to address cancer detection and classification applications via Raman spectroscopy and the development of nanoelectrochemical systems as suitable biosensors. The proposed technique utilizes a simpler but more advanced chemotaxonomic method for sensing cancer on monolayer graphene compared to previously reported methods. All previously reported methods involve complex protocols requiring the addition of various reagents along with the cancer cells. We believe our method can be further studied to establish an individual cancer index for recognizing every single cancer type.

EXPERIMENTAL METHODS

Materials. Synthetic chemicals were purchased from Alfa Aesar. Ferric chloride solution, nitric acid 19% solution, gold etchant (KI/I_2/DI water solution), copper etchant (Transene, CE-100), nickel etchant (Transene), and poly (methyl methacrylate) (2 wt % in chlorobenzene) were used in our experiment. For biological experiments, cancer cells were obtained from ATCC. RPMI-1640, phosphate buffer saline, and Trypsin-EDTA were purchased from Sigma-Aldrich, USA. Synthesis, transfer of graphene, and device fabrication were clearly described in our previous publication[26] and briefly explained in Supporting Information.

Sample Preparation for Raman Spectra Measurements. Colon carcinoma (CT-26), skin cancer (SCC-7), normal colon (CCD-841), kidney (HEK293), microglia (N9), liver (HepaRG), liver cancer (HepG2), breast cancer (MDAMB 231), breast cancer (MDAMB 468) cell lines are used in this experiment. SCC-7, CT-26, and MDAMB 468 cancer cells were suspended in a culture medium (RPMI-1640) and the number and viability of the cells were determined using a hemocytometer with trypan blue dye exclusion. The viability of cancer cells was over 95%. We cultured fresh cancer cells in a Petri dish in a 5% CO_2 atmosphere at 37 °C, grown to almost confluent and then passage by trypsin treatment. Cells were fixed in an ethanol dehydration train and used for experiment. For HEK293, N9, HepG2, HepaRG, and CCD-841 cells, Dulbecco's modified Eagle's medium was used. For MDAMB 231 cancer cells, the L-15 medium was used with only an O_2 atmosphere at 37 °C.

Raman Measurements. For the acquisition of the Raman spectra, a WITec Raman system was used with a grating of 1800/500 g mm^{-1}. For the source of excitation on the sample, a He−Ne 532 nm laser was used with a power of 70 μW. A 8 mm working distance, a 10× objective (Olympus) lens, and a 0.55 numerical aperture were used for recording the Raman spectra. A scanning area of 30 μm × 30 μm with 2−10 s acquisition time was applied to avoid laser damage to cancer cells.

Computational Method. First-principles calculations[38] were used to understand the bonding character of the constituents, those that are observed through Raman spectroscopy. Plane-waves (energy cutoff 40 Ry and charge density cutoff 240 Ry), generalized gradient approximation,[39] and ultrasoft pseudopotentials[40] with a suitable grid mesh (2 × 2 × 1)[41] were used for simulations. We computed

https://dx.doi.org/10.1021/acsabm.0c01377
ACS Appl. Bio Mater. 2021, 4, 1493−1498

dynamical matrices in the Brillouin zone using a perturbative linear response approach.[42]

■ ASSOCIATED CONTENT

Supporting Information

The Supporting Information is available free of charge at https://pubs.acs.org/doi/10.1021/acsabm.0c01377.

Graphene synthesis; transfer; device fabrication; physical characterization; and Raman spectra of top-gated monolayer graphene with cell lines (SCC-7, MDAMB 231, MDAMB 468, HepaRG, HepG2, CCD 841, HEK293, N9, and CT-26) (PDF)

■ AUTHOR INFORMATION

Corresponding Author

Dong Kee Yi − *Department of Chemistry, Myongji University, Yongin 03674, South Korea;* orcid.org/0000-0003-2604-9323; Email: vitalis@mju.ac.kr

Authors

Sitansu Sekhar Nanda − *Department of Chemistry, Myongji University, Yongin 03674, South Korea;* orcid.org/0000-0002-7663-4830

Sandeep Kaushal − *Department of Chemistry, Myongji University, Yongin 03674, South Korea*

Yong Shin − *Department of Biotechnology, Yonsei University, Seoul 03722, South Korea*

Kyusik Yun − *Department of Bionanotechnology, Gachon University, Seongnam 13120, South Korea*

Seong Soo A. An − *Department of Bionanotechnology, Gachon University, Seongnam 13120, South Korea*

K. P. S. S. Hembram − *Optoelectronic Materials and Devices Research Center, Korea Institute of Science and Technology (KIST), Seoul 02792, South Korea*

Georgia C. Papaefthymiou − *Department of Physics, Villanova University, Villanova, Pennsylvania 19085, United States*

Complete contact information is available at: https://pubs.acs.org/10.1021/acsabm.0c01377

Notes

The authors declare no competing financial interest.

■ ACKNOWLEDGMENTS

This work was supported by the Korean National Research Foundation (NRF-NRF, 2018R1A2B6007786).

■ REFERENCES

(1) Fasolino, A.; Los, J. H.; Katsnelson, M. I. Intrinsic Ripples in Graphene. *Nat. Mater.* **2007**, *6*, 858−861.

(2) Meyer, J. C.; Geim, A. K.; Katsnelson, M. I.; Novoselov, K. S.; Booth, T. J.; Roth, S. The Structure of Suspended Graphene Sheets. *Nature* **2007**, *446*, 60−63.

(3) Katsnelson, M. I. Graphene: Carbon in Two Dimensions. *Mater. Today* **2007**, *10*, 20−27.

(4) Geim, A. K.; Novoselov, K. S. The Rise of Graphene. *Nanoscience and Technology*, 2009, pp 11−19.

(5) Ohno, Y.; Maehashi, K.; Matsumoto, K. Label-Free Biosensors Based on Aptamer-Modified Graphene Field-Effect Transistors. *J. Am. Chem. Soc.* **2010**, *132*, 18012−18013.

(6) Yang, K.; Hu, L.; Ma, X.; Ye, S.; Cheng, L.; Shi, X.; Li, C.; Li, Y.; Liu, Z. Multimodal Imaging Guided Photothermal Therapy using Functionalized Graphene Nanosheets Anchored with Magnetic Nanoparticles. *Adv. Mater.* **2012**, *24*, 1867.

(7) Zhang, Y.; Nayak, T. R.; Hong, H.; Cai, W. Graphene: a versatile nanoplatform for biomedical applications. *Nanoscale* **2012**, *4*, 3833−3842.

(8) Kanakia, S.; Toussaint, J. D.; Chowdhury, S. M.; Lalwani, G.; Tembulkar, T.; Button, T.; Shroyer, K. R.; Moore, W.; Sitharaman, B. Physicochemical Characterization of a Novel Graphene-Based Magnetic Resonance Imaging Contrast Agent. *Int. J. Nanomed.* **2013**, *8*, 2821−2833.

(9) Markovic, Z. M.; Harhaji-Trajkovic, L. M.; Todorovic-Markovic, B. M.; Kepić, D. P.; Arsikin, K. M.; Jovanović, S. P.; Pantovic, A. C.; Dramićanin, M. D.; Trajkovic, V. S. In vitro Comparison of the Photothermal Anticancer Activity of Graphene Nanoparticles and Carbon Nanotubes. *Biomaterials* **2011**, *32*, 1121−1129.

(10) Russier, J.; León, V.; Orecchioni, M.; Hirata, E.; Virdis, P.; Fozza, C.; Sgarrella, F.; Cuniberti, G.; Prato, M.; Vázquez, E.; Bianco, A.; Delogu, L. G. Few-Layer Graphene Kills Selectively Tumor Cells from Myelomonocytic Leukemia Patients. *Angew. Chem.* **2017**, *56*, 3014−3019.

(11) Zanchetta, G.; Lanfranco, R.; Giavazzi, F.; Bellini, T.; Buscaglia, M. Emerging Applications of Label-free Optical Biosensors. *Nanophotonics* **2017**, *6*, 627−645.

(12) Karlsson, R.; Katsamba, P. S.; Nordin, H.; Pol, E.; Myszka, D. G. Analyzing a Kinetic Titration Series Using Affinity Biosensors. *Anal. Biochem.* **2006**, *349*, 136−147.

(13) Cooper, M. A. *Label-free Biosensors: Techniques and Applications*; Cambridge University Press, 2009.

(14) Cunningham, B. T.; Laing, L. G. Advantages and Application of Label-free Detection Assays in Drug Screening. *Expert Opin. Drug Discovery* **2008**, *3*, 891−901.

(15) Bellisola, G.; Sorio, C. Infrared Spectroscopy and Microscopy in Cancer Research and Diagnosis. *Am. J. Cancer Res.* **2012**, *2*, 1−21.

(16) Qian, X.; Peng, X.-H.; Ansari, D. O.; Yin-Goen, Q.; Chen, G. Z.; Shin, D. M.; Yang, L.; Young, A. N.; Wang, M. D.; Nie, S. In Vivo Tumor Targeting and Spectroscopic Detection with Surface-Enhanced Raman Nanoparticle Tags. *Nat. Biotechnol.* **2007**, *26*, 83−90.

(17) Jermyn, M.; Mok, K.; Mercier, J.; Desroches, J.; Pichette, J.; Saint-Arnaud, K.; Bernstein, L.; Guiot, M.-C.; Petrecca, K.; Leblond, F. Intraoperative Brain Cancer Detection with Raman Spectroscopy in Humans. *Sci. Transl. Med.* **2015**, *7*, 274ra19.

(18) Diamandis, E. P. Mass Spectrometry as a Diagnostic and a Cancer Biomarker Discovery Tool: Opportunities and Potential Limitations. *Mol. Cell. Proteomics* **2004**, *3*, 367−378.

(19) Atienzar, F. A.; Venier, P.; Jha, A. N.; Depledge, M. H. Evaluation of the Random Amplified Polymorphic DNA (RAPD) Assay for the Detection of DNA Damage and Mutations. *Mutat. Res.* **2002**, *521*, 151−163.

(20) Cheng, S.; Hideshima, S.; Kuroiwa, S.; Nakanishi, T.; Osaka, T. Label-Free Detection of Tumor Markers Using Field Effect Transistor (FET)-Based Biosensors for Lung Cancer Diagnosis. *Sens. Actuators, B* **2015**, *212*, 329−334.

(21) Loynachan, C. N.; Soleimany, A. P.; Dudani, J. S.; Lin, Y.; Najer, A.; Bekdemir, A.; Chen, Q.; Bhatia, S. N.; Stevens, M. M. Renal Clearable Catalytic Gold Nanoclusters for In vivo Disease Monitoring. *Nat. Nanotechnol.* **2019**, *14*, 883−890.

(22) Kong, K.; Kendall, C.; Stone, N.; Notingher, I. Raman spectroscopy for medical diagnostics — From In-vitro Biofluid Assays to In-vivo Cancer Detection. *Adv. Drug Delivery Rev.* **2015**, *89*, 121−134.

(23) Nijssen, A.; Schut, T. C. B.; Heule, F.; Caspers, P. J.; Hayes, D. P.; Neumann, M. H.; Puppels, G. J. Discriminating Basal Cell Carcinoma from its Surrounding Tissue by Raman Spectroscopy. *J. Invest. Dermatol.* **2002**, *119*, 64−69.

(24) Sha, M. Y.; Xu, H.; Natan, M. J.; Cromer, R. Surface-enhanced Raman Scattering Tags for Rapid and Homogeneous Detection of Circulating Tumor Cells in the Presence of Human Whole Blood. *J. Am. Chem. Soc.* **2008**, *130*, 17214−17215.

(25) Chan, J. W.; Taylor, D. S.; Zwerdling, T.; Lane, S. M.; Ihara, K.; Huser, T. Micro-Raman Spectroscopy Detects Individual Neoplastic and Normal Hematopoietic Cells. *Biophys. J.* **2006**, *90*, 648−656.
(26) Nanda, S. S.; Kim, B. J.; Kim, K.-W.; Nasir, T.; Park, J.; Yun, K.; Hembram, K. P. S. S.; Papaefthymiou, G. C.; Choi, J.-Y.; Yi, D. K. A New Device Concept for Bacterial Sensing by Raman Spectroscopy and Voltage-gated Monolayer Graphene. *Nanoscale* **2019**, *11*, 8528−8537.
(27) Wang, X.; Qian, X.; Beitler, J. J.; Chen, Z. G.; Khuri, F. R.; Lewis, M. M.; Shin, H. J. C.; Nie, S.; Shin, D. M. Detection of Circulating Tumor Cells in Human Peripheral Blood Using Surface-enhanced Raman Scattering Nanoparticles. *Cancer Res.* **2011**, *71*, 1526−1532.
(28) Keisham, B.; Cole, A.; Nguyen, P.; Mehta, A.; Berry, V. Cancer Cell Hyperactivity and Membrane Dipolarity Monitoring via Raman Mapping of Interfaced Graphene: Toward Non-invasive Cancer Diagnostics. *ACS Appl. Mater. Interfaces* **2016**, *8*, 32717−32722.
(29) Samanta, A.; Maiti, K. K.; Soh, K.-S.; Liao, X.; Vendrell, M.; Dinish, U. S.; Yun, S.-W.; Bhuvaneswari, R.; Kim, H.; Rautela, S.; Chung, J.; Olivo, M.; Chang, Y.-T. Ultrasensitive Near-infrared Raman Reporters for SERS-based In vivo Cancer Detection. *Angew. Chem.* **2011**, *123*, 6213−6216.
(30) Xia, J.; Chen, F.; Li, J.; Tao, N. Measurement of the Quantum Capacitance of Graphene. *Nat. Nanotechnol.* **2009**, *4*, 505.
(31) Yu, G. L.; Jalil, R.; Belle, B.; Mayorov, A. S.; Blake, P.; Schedin, F.; Morozov, S. V.; Ponomarenko, L. A.; Chiappini, F.; Wiedmann, S.; Zeitler, U.; Katsnelson, M. I.; Geim, A. K.; Novoselov, K. S.; Elias, D. C. Interaction Phenomena in Graphene seen through Quantum Capacitance. *Proc. Natl. Acad. Sci. U.S.A.* **2013**, *110*, 3282−3286.
(32) Téllez-Plancarte, A.; Haro-Poniatowski, E.; Picquart, M.; Morales-Méndez, J.; Lara-Cruz, C.; Jiménez-Salazar, J.; Damián-Matsumura, P.; Escobar-Alarcón, L.; Batina, N. Development of a Nanostructured Platform for Identifying HER2-heterogeneity of Breast Cancer Cells by Surface-enhanced Raman Scattering. *Nanomaterials* **2018**, *8*, 549.
(33) González-Solís, J. L.; Aguiñaga-Serrano, B. I.; Martínez-Espinosa, J. C.; Oceguera-Villanueva, A. Stage Determination of Breast Cancer Biopsy Using Raman spectroscopy and Multivariate Analysis. *AIP Conf. Proc.* **2011**, *1364*, 33−40.
(34) Nanda, S. S.; Kim, M. J.; Yeom, K. S.; An, S. S. A.; Ju, H.; Yi, D. K. Raman Spectrum of Graphene with its Versatile Future Perspectives. *TrAC, Trends Anal. Chem.* **2016**, *80*, 125−131.
(35) Prat, A.; Parker, J. S.; Karginova, O.; Fan, C.; Livasy, C.; Herschkowitz, J. I.; He, X.; Perou, C. M. Phenotypic and Molecular Characterization of the Claudin-low Intrinsic Subtype of Breast Cancer. *Breast Cancer Res.* **2010**, *12*, R68.
(36) Neve, R. M.; Chin, K.; Fridlyand, J.; Yeh, J.; Baehner, F. L.; Fevr, T.; Clark, L.; Bayani, N.; Coppe, J.-P.; Tong, F.; Speed, T.; Spellman, P. T.; DeVries, S.; Lapuk, A.; Wang, N. J.; Kuo, W.-L.; Stilwell, J. L.; Pinkel, D.; Albertson, D. G.; Waldman, F. M.; McCormick, F.; Dickson, R. B.; Johnson, M. D.; Lippman, M.; Ethier, S.; Gazdar, A.; Gray, J. W. A Collection of Breast Cancer Cell Lines for the Study of Functionally Distinct Cancer Subtypes. *Cancer Cell* **2006**, *10*, 515−527.
(37) Rouvray, D. H. The Search for Useful Topological Indices in Chemistry: Topological Indices Promise to have Far-reaching Applications in Fields as Diverse as Bonding Theory, Cancer Research, and Drug Design. *Am. Sci.* **1973**, *61*, 729−735.
(38) Giannozzi, P.; Baroni, S.; Bonini, N.; Calandra, M.; Car, R.; Cavazzoni, C.; Ceresoli, D.; Chiarotti, G. L.; Cococcioni, M.; Dabo, I.; Dal Corso, A.; de Gironcoli, S.; Fabris, S.; Fratesi, G.; Gebauer, R.; Gerstmann, U.; Gougoussis, C.; Kokalj, A.; Lazzeri, M.; Martin-Samos, L.; Marzari, N.; Mauri, F.; Mazzarello, R.; Paolini, S.; Pasquarello, A.; Paulatto, L.; Sbraccia, C.; Scandolo, S.; Sclauzero, G.; Seitsonen, A. P.; Smogunov, A.; Umari, P.; Wentzcovitch, R. M. QUANTUM ESPRESSO: a Modular and Open-source Software Project for Quantum Simulations of Materials. *J. Phys.: Condens. Matter* **2009**, *21*, 395502.
(39) Perdew, J. P.; Burke, K.; Ernzerhof, M. Generalized Gradient Approximation Made Simple. *Phys. Rev. Lett.* **1996**, *77*, 3865.
(40) Vanderbilt, D. Soft Self-consistent Pseudopotentials in a Generalized Eigenvalue Formalism. *Phys. Rev. B: Condens. Matter Mater. Phys.* **1990**, *41*, 7892.
(41) Monkhorst, H. J.; Pack, J. D. Special Points for Brillouin-zone Integrations. *Phys. Rev. B: Solid State* **1976**, *13*, 5188.
(42) Giannozzi, P.; Andreussi, O.; Brumme, T.; Bunau, O.; Buongiorno Nardelli, M.; Calandra, M.; Car, R.; Cavazzoni, C.; Ceresoli, D.; Cococcioni, M.; Colonna, N.; Carnimeo, I.; Dal Corso, A.; de Gironcoli, S.; Delugas, P.; DiStasio, R. A.; Ferretti, A.; Floris, A.; Fratesi, G.; Fugallo, G.; Gebauer, R.; Gerstmann, U.; Giustino, F.; Gorni, T.; Jia, J.; Kawamura, M.; Ko, H.-Y.; Kokalj, A.; Küçükbenli, E.; Lazzeri, M.; Marsili, M.; Marzari, N.; Mauri, F.; Nguyen, N. L.; Nguyen, H.-V.; Otero-de-la-Roza, A.; Paulatto, L.; Poncé, S.; Rocca, D.; Sabatini, R.; Santra, B.; Schlipf, M.; Seitsonen, A. P.; Smogunov, A.; Timrov, I.; Thonhauser, T.; Umari, P.; Vast, N.; Wu, X.; Baroni, S. Advanced Capabilities for Materials Modelling with Quantum ESPRESSO. *J. Phys.: Condens. Matter* **2017**, *29*, 465901.

https://dx.doi.org/10.1021/acsabm.0c01377
ACS Appl. Bio Mater. 2021, 4, 1493−1498